FOLLOWING DYNAMICS OF PROTEIN/NUCLEIC ACID INTERACTIONS IN REAL-TIME

by

Min Sun Kim

B.S., Yonsei University, 1999

M.S., Yonsei University, 2001

Submitted to the Graduate Faculty of

Medicine in partial fulfillment

of the requirements for the degree of

Master of Science

University of Pittsburgh

2008

UNIVERSITY OF PITTSBURGH

SCHOOL OF MEDICINE

This thesis was presented

by

Min Sun Kim

It was defended on

November 21, 2007

and approved by

Saleem Khan, PhD, Department of Microbiology and Molecular Genetics

Ronald Wetzel, PhD, Department of Structural Biology

Richard Steinman, MD, PhD, Department of Medicine and Pharmacology

Judith Klein-Seetharaman, PhD, Department of Structural Biology

Thesis Advisor: Sanford Leuba, PhD, Department of Cell Biology and Physiology

FOLLOWING DYNAMICS OF PROTEIN/NUCLEIC ACID

INTERACTIONS IN REAL-TIME

Min Sun Kim, M.S.

University of Pittsburgh, 2008

Abstract.

Methyl-CpG binding protein 2 (MeCP2) is a protein associated with transcriptional repression of other proteins and its various mutants are found in Rett syndrome patients, which is a severe neurodevelopmental disease found in 1/15,000 females. It has specific binding affinity to methyl-CpG domain but also binds to architectural DNA structure. Here, its binding dynamics to Holliday junction structure was investigated by using single molecular detections; scanning confocal fluorescence microscope and wide-field evanescent field fluorescence microscope. Through these studies, we could distinguish the difference of transitions of the substrate with and without MeCP2. The effect of this MeCP2 binding to 4WJ will be discussed in terms of the structures and transition times.

TABLE OF CONTENTS

LIST OF FIGURES

1.0 INTRODUCTION

1.1 BACKGROUND AND SIGNIFICANCE

1.1.1 General background

Rett Syndrome (RTT) is a severe childhood neurodevelopmental disorder found in 1/15,000 females [1-3]. The symptoms of this disease are similar to those of Angelman syndrome and autism. RTT patients show stereotypic and repetitive hand motions, cognitive impairment, problems with socialization, loss of verbal skills, and so forth [4-7]. The cause of this syndrome is the various mutations in methyl-CpG binding Protein 2 (MeCP2) [8-15].

MeCP2 has two functional domains, the methyl-CpG binding domain (MBD) and the transcriptional repression domain (TRD) [16-18]. It binds to methylated CpG dinucleotides [19-21] and represses transcriptions [22-23], so that it can prevent expression of certain proteins when they are not needed. Because of this affinity to methylated CpG domain, DNA methylation can inhibit transcription of chromatin template by ~50-fold, beyond the 50-fold repression caused by organizing naked DNA into chromatin structure [24-26]. MeCP2 competes with DNA architectural binding protein such as linker histone H1 [26], so that it can bind to nucleosomes and Holliday junctions even though there is no methylated CpG domain. Besides, point mutations in MeCP2 are associated with Rett Syndrome. Thus, it is important to study dynamics

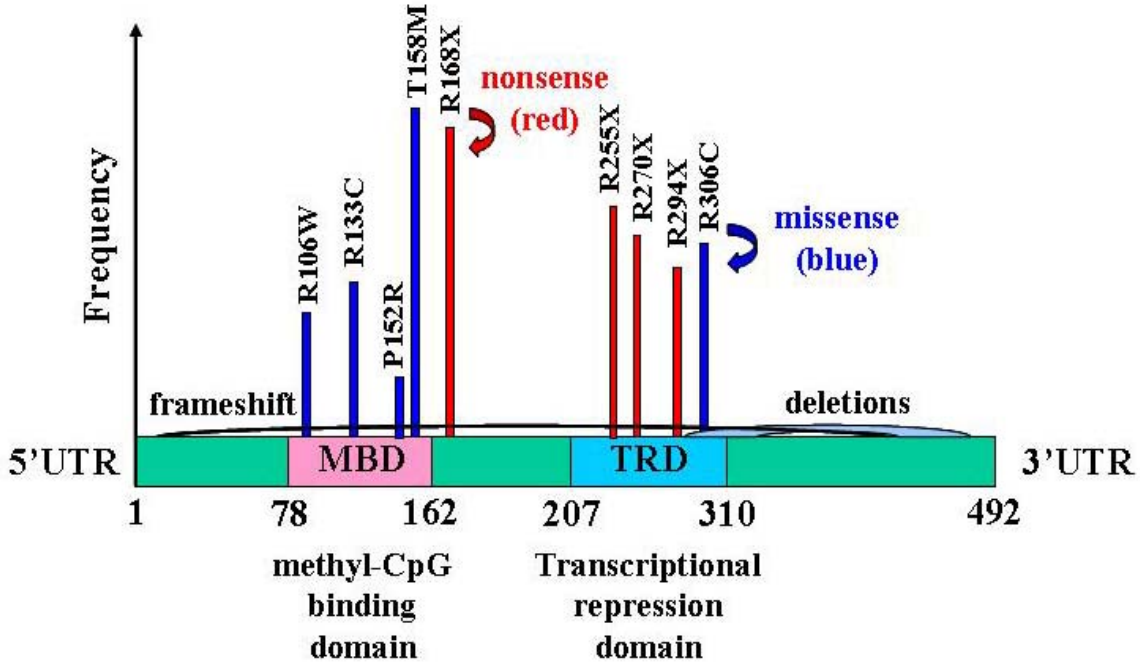

Figure 1. Hotspots of mutations identified in Rett Syndrome patients.

of MeCP2/DNA interactions. Figure 1 shows the possible mutations of MeCP2 found in RTT patients and their frequencies. Among those mutants, R306C mutant was used for my experiment.

1.1.2 Single Pair Fluorescence Resonance Energy Transfer (spFRET)

Single pair fluorescence energy transfer (spFRET) is a good experimental method to study kinetics of motion in 2-10 nm scale [27-31]. At the same time population study is also possible. Thus, I used Holliday Junction as a substrate, which has 11 base pairs for each arm and whose two separate ends are labeled with two dyes, a donor and an acceptor, so that they can be in previously mentioned distance range. It will be named as 4WJ afterwards. Figure 2 shows the basic concept of spFRET and its typical signal in time. If the distance between two dyes, a donor and an acceptor, is in 2-10 nm and donor dyes are excited, the excited donors can transfer their excessive energy to their neighboring acceptors and excite them. Then, we can observe the fluorescence from acceptor dyes. The energy transfer efficiency is inversely proportionate to the R^6, when R is the distance between dyes, and usually shows a big change around 4-6nm distance. For this energy transfer, there should be large spectral overlap between donor emission and acceptor absorption spectra as well. This is the reason that I used Cy3 and Cy5 dyes as a donor and an acceptor, respectively [32]. In spFRET experiments, fluorescence intensities of Cy3 and Cy5 are anticorrelated with each other. An example of typical spFRET time trajectory is shown in Figure 2.

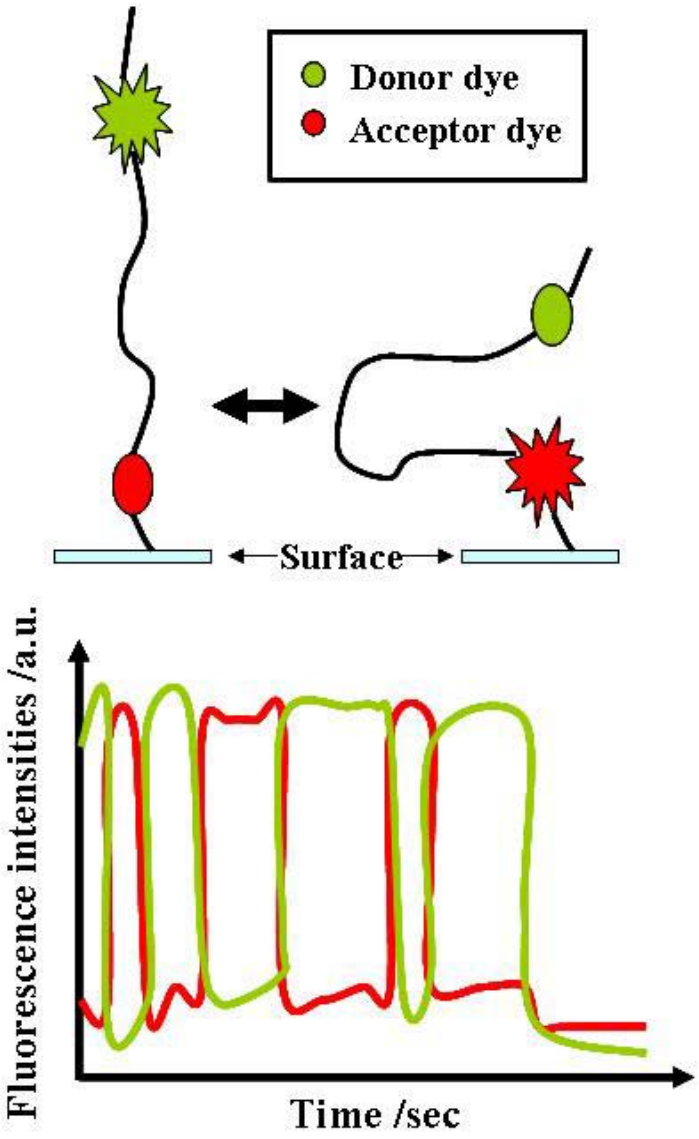

Figure 2. The principle of spFRET (top) and an example fluorescence time trajectories of donor and acceptor dyes

2.0 EXPERIMENTALS

2.1 SAMPLE PREPARATION

2.1.1 Hybridization of DNA substrate

As described in previous section shortly, 4WJ used as a substrate for my experiments were assembled with four oligonucleotides of given sequences whose core doesn't allow the branch migration (shown in Figure 3) [30]; 5'-Cy5-CCC TAG CAA GCC GCT GCT ACG G, 5'-Cy3-CCG TAG CAG CGC GAG CGG TGG G, 5'-Biotin-CCC ACC GCT CGG CTC AAC TGG G, and 5'-CCC AGT TGA GCG GTT GCT AGG G. All of these oligonucleotides were synthesized using phosphoramidite chemistry implemented on DNA synthesizer (IDTDNA.com).

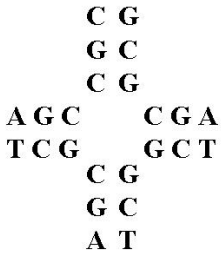

Figure 3. DNA sequence of the center of junction.

Each oligonucleotide was dissolved into 100 μM water solution. I mixed 15 μL of each solution and 5 μL of 10X assembly buffer (100 mM Tris-HCl, pH 7.5, 500 mM NaCl, and 10 mM EDTA) together, heat it up to 65 °C, left it for few minutes, and slowly cooled it down to 37 °C over several hours to hybridize. And then I checked its formation using the 1% agarose gel in 0.5X TAE buffer.

2.1.2 Preparation of flow cells

The flow cell was constructed on a cleaned quartz slide (3 in by 1 in) with two holes (1mm diameter) on its diagonal. To clean quartz slide, first, it was placed in 30% detergent solution and sonicated for an hour followed by wash and 5-15 min of sonication in water, Acetone, ethanol, and 1M KOH. Parafilm with a channel of a few millimeters wide and ~5 centimeter long was used for spacing between quartz slide and a glass coverslip. Then, 30 μL of 1 mg/ml streptavidin (Roche) solution in T50 buffer (10 mM Tris-HCl, pH 7.5, and 50 mM NaCl) was injected, and washed out 10 min later to allow them to be adsorbed onto the cell surface, so that biotinylated DNA were immobilized on the surface [33]. In order to prevent oxygen quenching, the imaging buffer was added right before imaging, which contained 0.4% glucose, 1% β-mercaptoethanol, glucose oxidase and catalase (Roche) [34].

2.2 EXPERIMENTAL SET_UPS

2.2.1 Scanning Confocal Fluorescence Microscope (SCFM)

Scanning confocal fluorescence microscope (SCFM) [30, 35-39] was used to measure the real-time dynamics of single molecules, which is a single 4WJ substrate, by spFRET of the cyanine dyes, Cy3 and Cy5. Figure 5 shows the experimental SCFM set-up. The excitation light is passing through an expander, which increase the beam diameter to fill the back aperture of the objective. In turn, a dichroic mirror reflects this beam into the high numerical aperture (NA) objective. And then, backscattered fluorescence from sample is collected by the same objective, passes through the dichroic mirror, reflected by flip mirror, and separated into a donor and an acceptor signals by additional dichroic mirror. Finally, it is focused onto the single-photon sensitive avalanche photodiode detector (APD). In detail, the 532 nm laser beam by a miniature solid-state diode pumped laser module (GM32-5SL) from Intelite Inc. was delivered via single mode fiver through a collimating lens and a pinhole and a dichroic mirror was placed the back end of a 60X 1.2 NA water immersion objective to illuminate the sample in the quartz cell. Since a single objective lens is used for both illumination of incident light and collection of the sample emission in SCFM system, it is important to pick a proper objective. In order to collect more emission signal and reject background well, the larger NA of objective is the better. Both dichroic mirrors and filters were purchased from Chroma Technology Corp. A Z532RDC-532 nm dichroic mirror, the one closer to excitation light source, separates the fluorescence signal from the incident light, and the other one, 620DCXR-620 nm dichroic mirror, separates the Cy3 and Cy5 signals into two channels. Two filters right before each APD are HQ585-70M band pass filter to filter out the donor signal and E645LP long pass filter to filter out the acceptor signal.

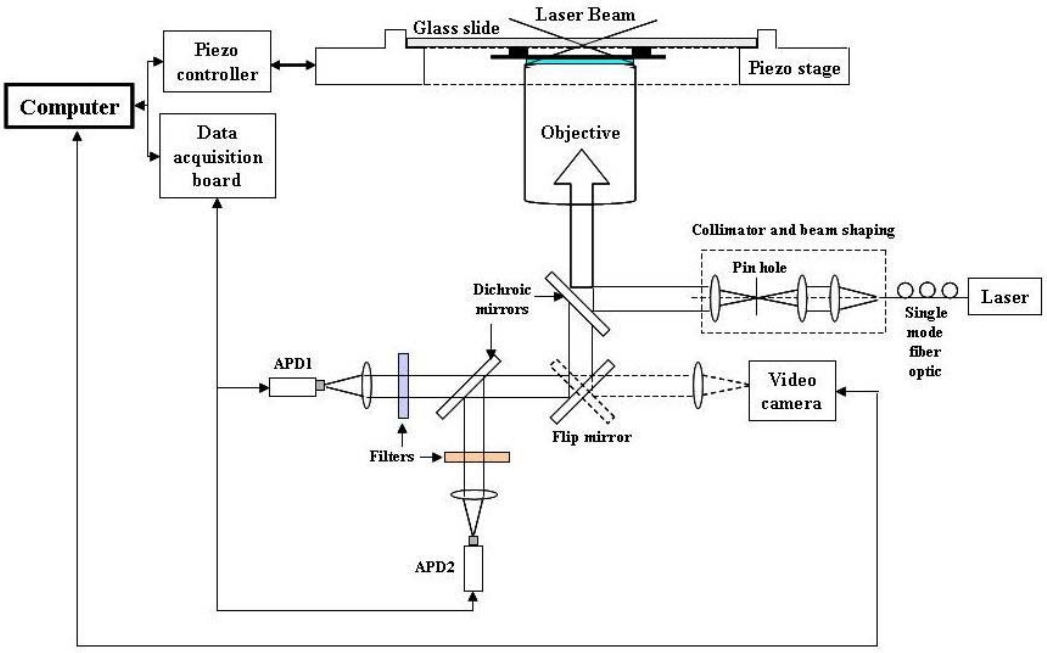

Figure 4. Schematic drawing of the SCFM set-up.

The APDs were SPCM-AQR-15 from Perkin Elmer Life Science. They are self-contained modules that detect single photons from 400 to 1060 nm, so that this wavelength range can cover the entire emission spectra of both Cy3 and Cy5 dyes. There are two ways of scanning; one is that incident light moves on the flow cell, and the other is that the whole sample stage moves on the fixed, focused light. For the convenience of system control, I used the latter one, so that I could fix most of optics at certain position and get better reproducibility of focusing. The Physik Instrument stage (PI P-527.2CL) was used for this set-up. It can scan a range of 200 μm × 200 μm × 50 μm and has 66 mm × 66mm clear aperture where I can place the flow cell. With this piezo stage, it is possible to scan the sample with nm resolution in x- and y-directions. Simultaneously collected fluorescence signals from Cy3 and Cy5 by two separate APDs after filters were imaged and analyzed by the algorithms developed by Haocheng Zheng. With this program, I scanned 10 μm × 10 μm of single molecules with a resolution of 0.1 μm per pixel and the integration time was 10 msec/pixel.

2.2.2 Wide-field Prism-based Evanescent Field Fluorescence Microscope (wide-field EFFM)

Our wide-field prism-based evanescent field fluorescence microscope (wide-field EFFM) [40-42] was built on the basis of the inverted fluorescent microscope (IX-71, Olympus) with 60X 1.2-NA water immersion objective (Olympus). Diode-pumped, ultra compact, 532-nm Green Laser (CrystaLaser) was used as a excitation light source. Using a Galilean beam expander, 10X (Newport), the beam diameter was increased. Via a couple of beam directing mirrors, 25.0 mm diagonal, H32-945 (Edmund Optics), the light was guided to the focusing lens. By adjust this lens, a circularly polarized beam was focused on the small pellin broca prism PLBC-5.0-79.5-ss

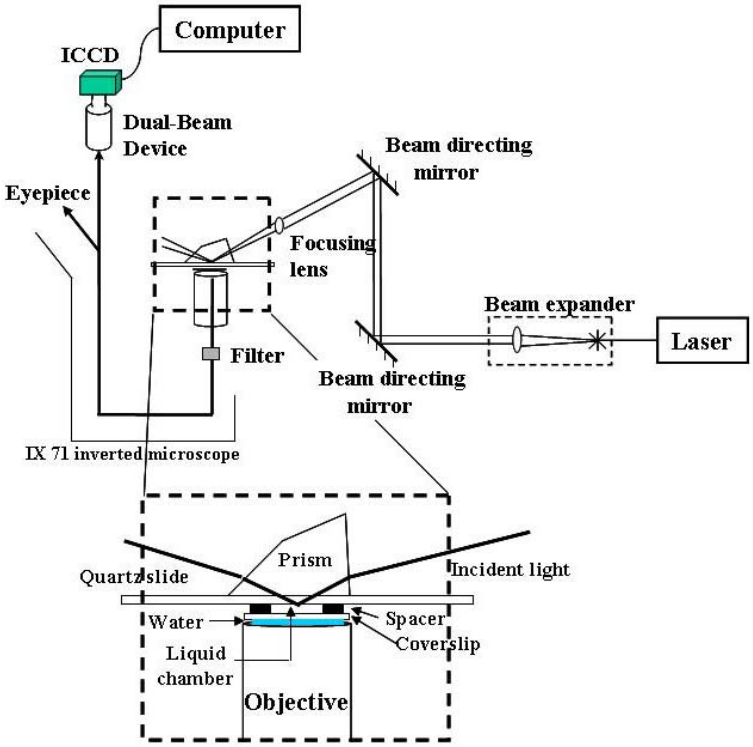

Figure 5. Schematic of the evanescent filed fluorescence microscope (EFFM).

(CVI Laser) with an angle of 65.7º [40] placed on the flow cell mediated by a drop of fluorescent –free oil (Cargille type FF, Fisher Scientific) for optical connection, so that I could get the total internal reflection at the surface and an exponentially decaying evanescent field through the flow cell. This flow cell was first placed on the previously mentioned water immersion objective. The fluorescence signal collected through the objective passed a Dual-view (Optical Insights) filter set system that would separate Cy3 and Cy5 signals into a two-part image on the intensified charge coupled device (ICCD) camera (I-PentaxMAX, Princeton Instruments). With this Dual-view, a dichroic 610DCLP, Cy3 band-pass D580-40 filter and a long-pass E645 filter (Chroma) were used for the Cy3 and the Cy5, respectively. As a result, I can record movies of two identical areas of 100 μm × 200 μm, one on the left presents Cy3 signals and on the right the corresponding Cy5 signals on the same area.

3.0 RESULTS AND DISCUSSIONS

3.1 MECP2 BINDING TO ARCHTECTURAL DNA STRUCTURE, 4WJ

The fact that MeCP2 binds to nucleosome structure and displace linker histone H1 has been already known. I assumed that it would also bind to the 4WJ structure because it has similar the part of nucleosomal structure where H1 binds and H1 binds to this substrate as well. Thus, I will first show the binding of MeCP2 to 4WJ, and then elucidate the dynamics of this DNA/protein interaction comparing with that of the naked 4WJ.

I used a 1% agarose gel to see if MeCP2 binds to 4WJ. As seen in Figure 6, there was a shift when MeCP2 was added. MeCP2 R306C mutant also bound to this substrate.

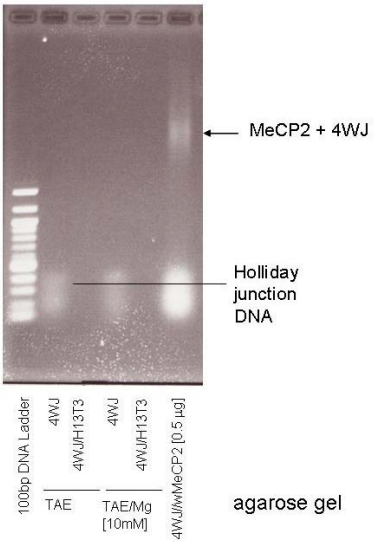

Figure 6. Gel shift.

In parallel, I tried to improve the experimental condition to get longer lasting, non-bleaching signals for longer observation.

3.2 SINGLE MOLECULAR DITECTION OF SINGLE PAIR FRET WITH SCFM

3.2.1 Data and results for the naked 4WJ molecule

Figure 7 describes how 4WJ molecules flip-flop between two different conformations. One on the left corresponds to low FRET state, which means the distance between two dyes is relatively long so that the amount of energy transferred from a donor molecule to the neighboring acceptor molecule is less. On the other hand, more energy can be transferred in the state on the right which is called high FRET state because of the shorter distance between dyes. From this model, I could expect that the transition between two distinct FRET states would be observed. And it turned out to be true. A graph on top left corner in Figure 8 is a typical time trajectories of Cy3 and Cy5 fluorescence signals from a single molecule. In order to get this time trace, I first scanned 10 μm × 10 μm areas then I could see tens of red and green dots from a single scan. Among those dots, I looked for red dots which neighbored with only one green dot and those pairs shouldn't have any other dyes around because they might interfere with each other. I clicked them and recorded a time trace of each donor-acceptor pair one by one. I repeated this procedure until I got over hundred traces. For data analysis, these time traces in fluorescence intensities were converted to the apparent efficiency of FRET (E_{app}) in time domain. Equation 1 shows how to convert [31].

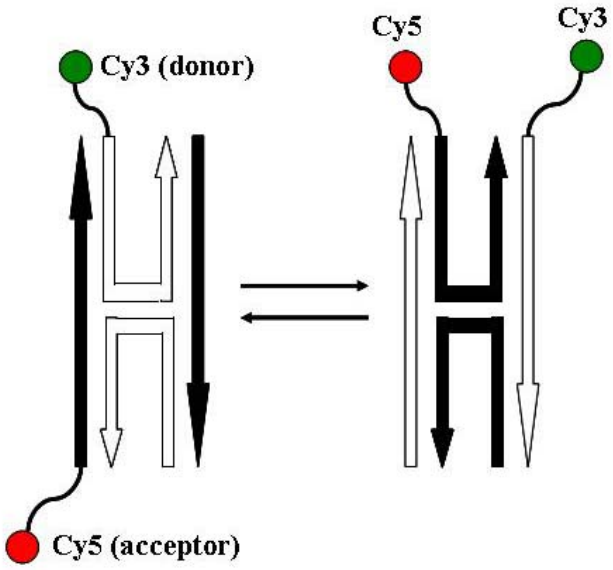

Figure 7. A structure of 4WJ substrate with two dyes and possible conformations.

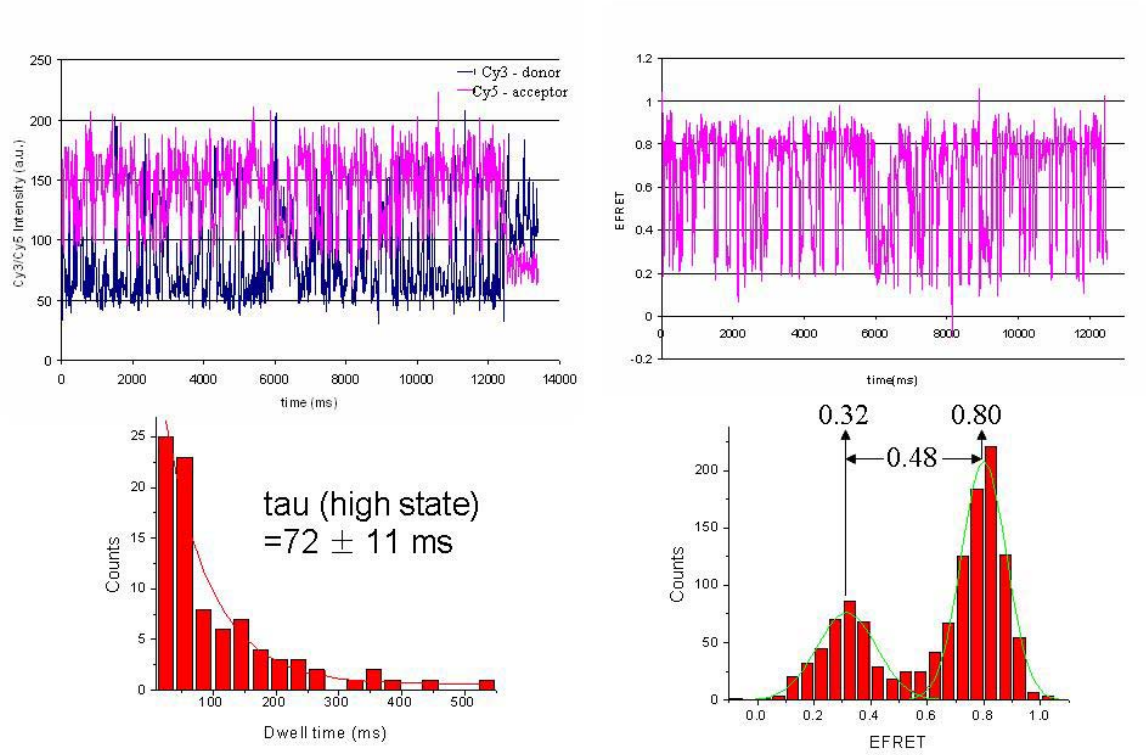

Figure 8. Typical FRET data from 4WJ. Time trajectories and apparent EFRET of a single molecule, and apparant EFRET distribution and histogram of dwell time in high FRETstate (clockwise from the top left).

$$E_{app} = \frac{I_{cy5}-I_{cy5,background}-0.1*(I_{cy3}-I_{cy3,background})}{\{I_{cy5}-I_{cy5,background}-0.1*(I_{cy3}-I_{cy3,background})\}+(I_{cy3}-I_{cy3,background})}$$

Equation 1. Equation to calculate apparent efficiency of FRET (E_{app}).

The apparent EFRET is defined as the ratio of the fluorescence intensity of an acceptor dye to the total amount of fluorescence from both a donor and an acceptor dyes. Since the excitation beam wavelength is at 532 nm, it can only excite donor dyes but not acceptors. It means that the apparent EFRET is the ratio of the amount of energy transferred to acceptor dye to the total amount of energy that was absorbed. But fluorescence intensities of Cy3 and Cy5 have to be corrected by subtraction of their background signals and even cross-talk from donor signal for Cy5. Again, it is clear that two distinct FRET states exist and the transition between these two states keeps occurring. Next, I did population studies. First of all, apparent EFRET distribution was plotted over all tens of molecules. This distribution plot was well fitted with the sum of two Gaussian peaks whose maximum positions (0.32 and 0.80) are similar to the apparent EFRET values of high and low states calculated for the individual traces. And their difference is about 0.48. For the last, dwell time analysis was done. Dwell time is defined as the time length during which the conformation of the molecule remains in one state. In order to measure dwell times, a proper threshold was manually set up in the middle of low and high FRET. The number of points was counted when the FRET was lower and higher than this threshold and then multiplied by the integration time which was 10 msec in my experiment. All the dwell times for every molecule were plotted together as a histogram and it was fitted with single exponential decay curve. Calculated decay time from this fitting corresponds to the average dwell time of each state which is in inverse proportion to transition rate constant. The obtained dwell time in high state was about 70 msec. That of in low state is not shown but the value was little less than that of high state.

3.2.2 Data and results for the complex of MeCP2 and 4WJ molecule

In order to see the effect of MeCP2 binding on the DNA flip-flop, MeCP2 stored in the buffer that contained 10 mM Tris-HCl, pH 7.5, 150 mM NaCl, and 50 % glycerol was added to the imaging buffer, waited for several minutes for binding, and then imaged. Data collection and analysis were done exactly in the same way which was used for study of naked 4WJ dynamics. The result is shown in Figure 9. The obtained values for the MeCP2 bound 4WJ would be listed; the average apparent efficiencies of FRETs of low and high states were 0.37 and 0.74, respectively, so that the difference between them was 0.37, and the averaged dwell time in high state was about 40 msec and that in low state was little less.

3.2.3 Comparison of the result for the MeCP2/4WJ complex with that for naked 4WJ

It is possible to see the changes in apparent efficiencies of FRETs from the individual plots in time domain. But I will simply compare the obtained numbers from the fitting in population studies. The average apparent efficiencies of FRET in low FRET state gets higher from 0.32 to 0.37 when MeCP2 was added and that in high FRET state gets lower from 0.80 to 0.74. Thus, the difference becomes smaller from 0.48 to 0.37. It means that the conformational changes occur in shorter distance range. Another parameter which can be compared is dwell time. Dwell time in high state decreased from 72 msec to 42 msec, which means that the transition between the conformations got faster. Because the transition rate is proportionate to decaying time inversely, the shorter decaying time corresponds to the higher transition rate and it will end up on the faster transition. For convenience, I made a plot of dwell time in high state as a function of the apparent efficiencies of FRET peak separation, apparent EFRET difference between high and

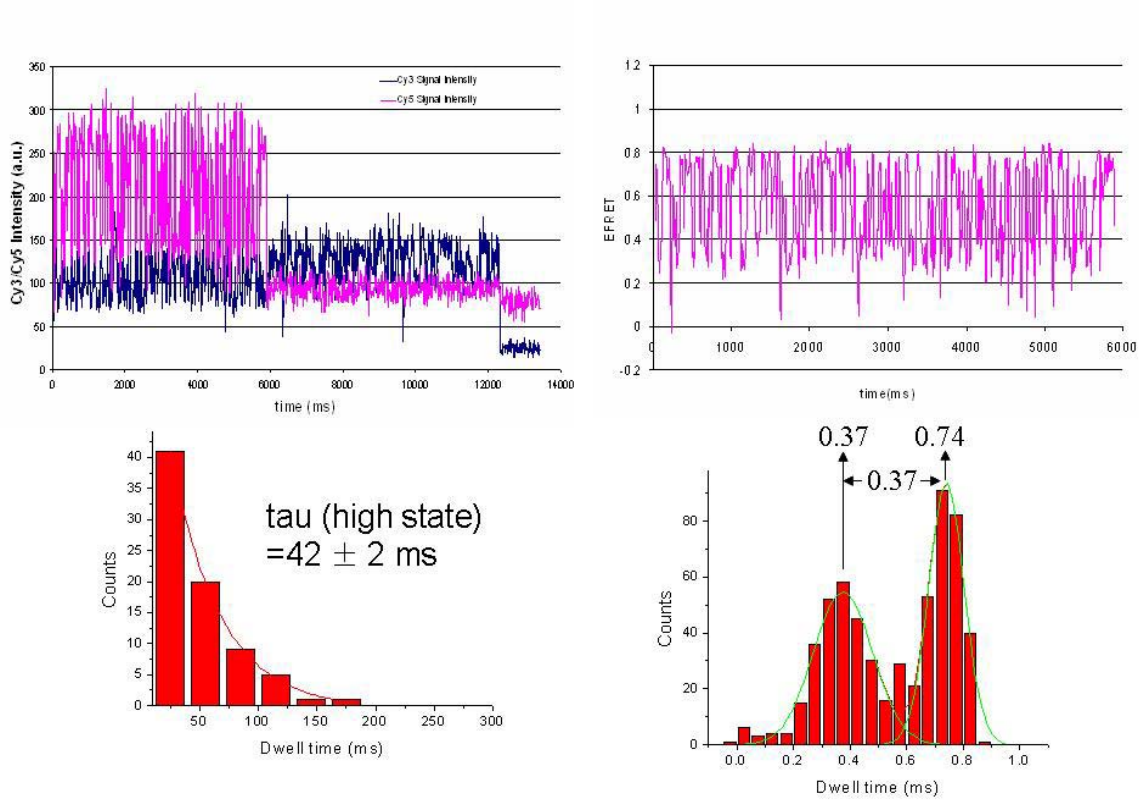

Figure 9. Typical FRET data from MeCP2 bound 4WJ. Time trajectories and apparent efficiencies of FRET of a single molecule, and histogram of dwell time in high FRET state and distribution of the apparent efficiencies of FRET (clockwise from the top left).

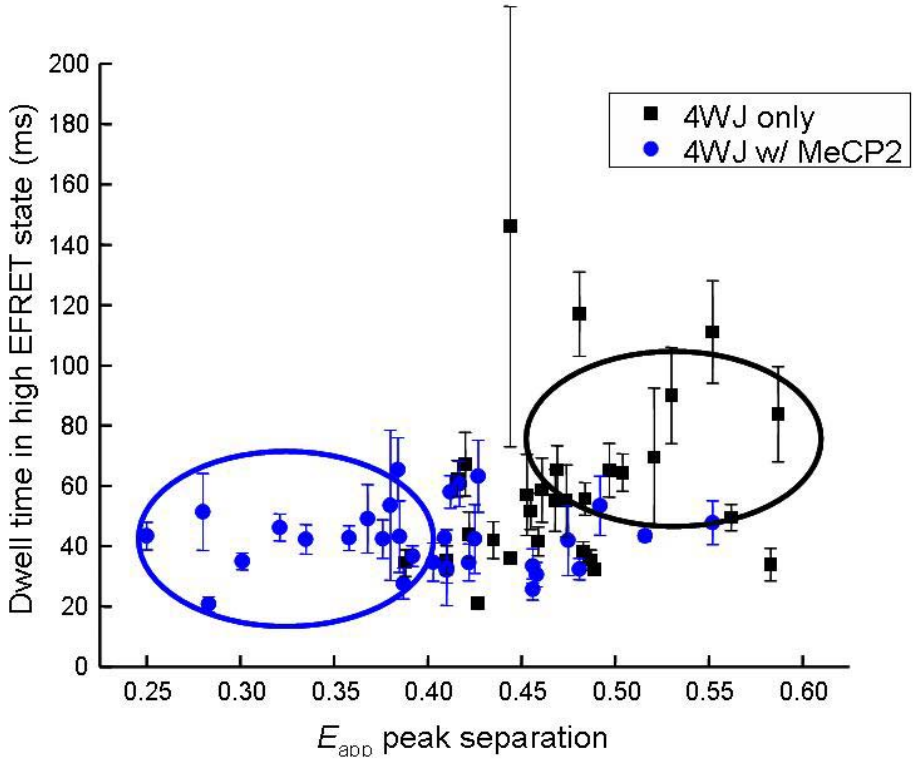

Figure 10. The plot of dwell times in high FRET state versus the apparent efficiencies of FRET peak separations.

low state. Each dot (circle or square) drawn with error bar corresponds to a single molecule. Those with huge error bar are from the early photobleached molecules so that they don't have much data points. In this plot, blue dots representing the 4WJ molecules interacting with MeCP2 are mainly crowded in the bottom left corner of the graph relatively. Thus, it is concluded that MeCP2 binding on the 4WJ will restrict the range of flip-flop a bit but accelerate the transition. Figure 11 depict this result. If the transition of naked 4WJ occurred from stacked X-structure to another stacked X-structure, then that of 4WJ interacting with MeCP2 would occur from more-opened structure to another one. That is, if the conformers of naked 4WJ were in high and low FRET states, then those of 4WJ/MeCP2 complex would be in medium high and medium low states.

3.3 SINGLE MOLECULAR DITECTION OF SINGLE PAIR FRET WITH SCFM

SCFM set-up itself has great advantage of high resolution in both space and time and high signal-to-noise ratio (S/N ratio). But to record individual traces, I have to assign the position of molecule, which I want to scan, one by one, so that simultaneous recording of multiple traces is impossible. It limits the type of experiment that this set-up can be applied to. For example, it is not possible to inject certain molecule that interacts with substrate in the middle of scanning to see the change in one trace. In this sense, it would be very useful if the resolution and time response of wide-field EFFM could be improved close to the level of SCFM. Fortunately, we modified wide-field EFFM with a new camera, a back-illuminated electron-multiplying CCD, recently. It has faster response and higher sensitivity than our previous set-up. As a result, I was able to go down to 15 msec binning time but still have good quality of data.

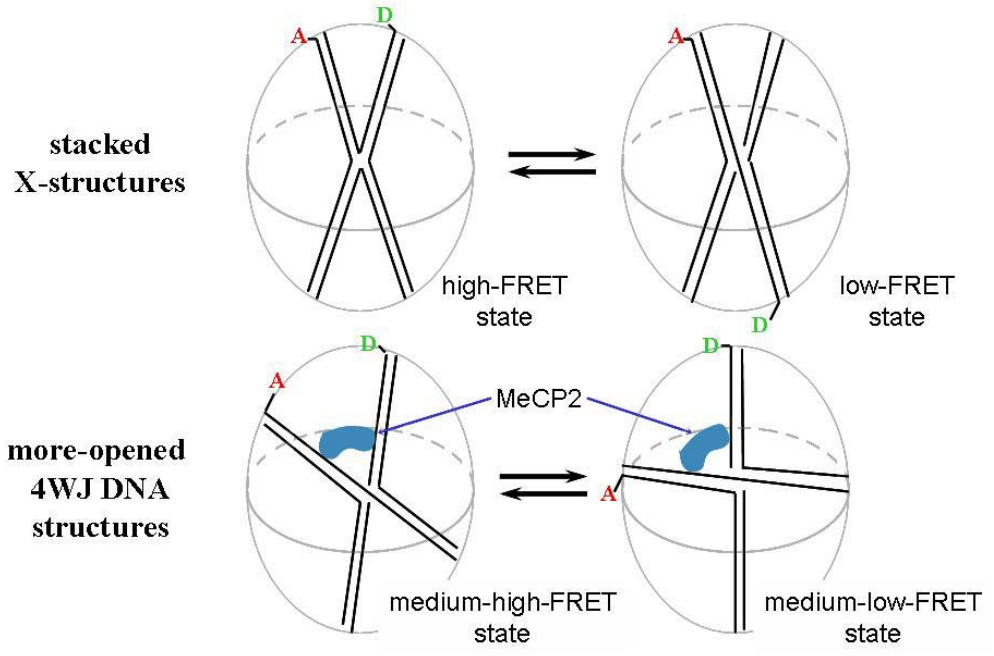

Figure 11. Description of the flip-flop dynamics of 4WJ with and without MeCP2.

Next problem to be solved will be blinking and photobleaching. So far, I have removed those regions manually before data analysis. Recent reports show that Trolox is used instead of β-mercaptoethanol in imaging buffer and gives longer lasting, non-bleaching FRET signals [43-44]. Advantage of using Trolox is that 2 mM solution or even less can replace the effect of 143 mM β-mercaptoethanol and gives better signals. Since Trolox has a similar structure to Vitamin E, I tried to use not only Trolox but also a couple of other Vitamin E analogues, which are more easily soluble. But there was no effect observed with these analogues. I record the movies with our improved wide-field EFFM set-up using 2 mM Trolox instead of β-mercaptoethanol. Figure 12 shows the result. 4WJ was used as a substrate again. And the binning time was 15 msec. The FRET signal lasts over 30 sec without blinking and photobleaching. Then, I tried to record longer movies for a couple of minutes to see how long it takes until photobleaching. However, because of the huge increase of number of frames, it couldn't be stored. But it is still important to look for the condition which makes longer movie recording possible, so further experiment has to be done by adjust resolution, recording time, and other factors.

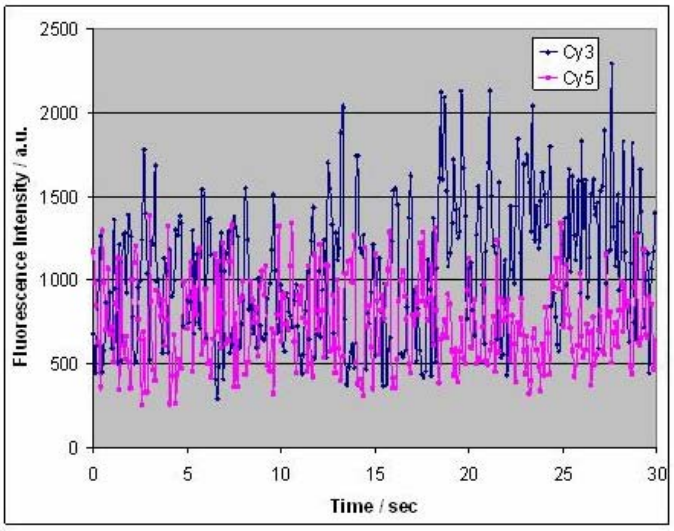

Figure 122. A time trajectory of 4WJ using Trolox as a part of imaging buffer.

4.0 SUMMARY

Rett Syndrom (RTT) is a severe childhood neurodevelopmental disorder found in 1/15,000 females. And the cause of this syndrome is the various mutations in methyl-CpG binding Protein 2 (MeCP2), which is involved with transcriptional repression of other protein. Since it competes with DNA architectural binding protein like H1, the dynamic of its binding needs to be investigated. It was observed in time domain by single molecular detections; SCFM and wide-field EFFM. As a simple model system, 4WJ was used, which typically shows flip-flop between two stacked X-structures. Its high and low apparent EFRET are 0.80 and 0.32 and its high state dwell time is 72 msec. However, when it interacts with MeCP2, the high EFRET gets lower to 0.74, the low EFRET gets higher to 0.37, and the high dwell time becomes shorter. Conclusively, binding of MeCP2 to 4WJ interrupt free flip-flop motion of 4WJ, so it cannot form the stacked X-structures but stays in more-opened structure. For better comparison, the experiment needs to be repeated with wild type MeCP2 and further effort to get longer observation is also required.

REFERENCES

1. Glaze, D. G. Ment. Retard. Dev. Disabil. *Res. Rev*., **2004**, *10*, 154

2. Neul, J. L.; Zoghbi, H. Y. *Neuroscientist*, **2004**, *10*, 118

3. Zoghbi, H. Y. *Science*, **2003**, *302*, 826

4. Skjeldal, O. H.; Tetzchner, S. von; Jacobsen, K.; Smith, L. *Neuropediatrics*, **1995**, *26*, 87

5. Zappella, M. *Eur. Child Adolsec. Psychiatry*, **1994**, *3*, 52

6. Zappella, M. *Eur. Child Adolsec. Psychiatry*, **1997**, *6*, 23

7. Zappella, M.; Gillberg, C.; Ehlers, S. *J. Autism Dev. Disord.* **1998**, *28*, 519

8. Huppke, P.; Laccone, F.; Kramer, N.; Engel, W.; Hanefeld, F. *Hum. Mol. Genet.* **2000**, *9*, 1369

9. Bienvenu, T.; Carrie, A.; Roux, N. de; Vinet, M. C.; Jonveaux, P.; Couvert, P.; Villard, L.; Arzimanoglou, A.; Beldjord, C.; Fontes, M.; Tardieu, M.; Chelly, J. *Hum. Mol. Genet.* **2000**, *9*, 1377

10. Cheadle, J.; Gill, H.; Fleming, M.; Maynard, J.; Kerr, A.; Leonard, H.; Krawczak, M.; Cooper, D. N.; Lynch, S.; Thomas, N.; Hughes, H.; Hulten, M.; Ravine, D.; Sampsom, J. R.; Clarke, A. *Hum. Mol. Genet.* **2000**, *9*, 1119

11. Bona, C. De; Zappella, M.; Hayek, G.; Meloni, I.; Vitelli, F.; Bruttini, M.; Cusano, R.; Loffredo, P.; Longo, I.; Renieri, A. *Eur. J. Hum. Genet.* **2000**, *8*, 325

12. Laccone, F.; Huppke, P.; Hanefeld, F.; Meins, M. *Hum. Mutat*, **2001**, *17*, 183

13. Nielsen, J. B.; Henriksen, K. F.; Hansen, C.; Silahtaroglu, a.; Schwartz, M.; Tommerup, N. *Eur. J. Hum. Genet.* **2001**, *9*, 178

14. Renieri, A.; Meloni, I.; Longo, I.; Ariani, F.; Mari, F.; Pescucci, C.; Cambi, F. *J. Mol. Med.* **2003**, *81*, 346

15. Amir, R. E.; Veyver, I. B. Van den; Wan, M.; Tran, C. Q.; Francke, U.; Zoghbi, H. Y. *Nat. Genet.* **1999**, *23*, 185

16. Wakefield, R. I. D.; Smith, B. O.; Nan, X.; Free, A.; Soteriou, A.; Uhrin, D.; Bird, A.; Barlow, P. N. *J. Mol. Biol.* **1999**, *291*, 1055

17. Ohki, I.; Shimotake, N.; Fujita, N.; Nakao, M.; Shirakawa, M. *EMBO J.* **1999**, *18*, 6653

18. Ohki, I.; Shimotake, N.; Fujita, N.; Jee, J.-G.; IkeGami, T.; Nakao, M.; Shirakawa, M. *Cell*, **2001**, *105*, 487

19. Meehan, R. R.; Lewis, J. D.; Bird, A. P. *Nucleic Acids Res.* **1992**, *20*, 5085

20. Lewis, J. D.; Meehan, R. R.; Henzel, W. J.; Maurer-Fogy, I.; Jeppesen, P.; Klein, F.; Bird, I. P. *Cell*, **1992**, *69*, 905

21. Koch, R. J.; Bird, I. P. *Biochemistry*, **2004**, *43*, 5011

22. Matarazzo, V.; Cohen, D.; Palmer, A. M.; Simpson, P. J.; Khokhar, B.; Pan, S.-J.; Ronnett, G. V. *Mol. Cellular Neuroscience*, **2004**, *27*, 44

23. Nan, Z.; Campoy, F. J.; Bird, A. *Cell*, **1997**, *88*, 471

24. Bird, A. P.; Wolffe, A. P. *Cell*, **1999**, *99*, 451

25. Georgel, P. T.; Horowitz-Scherer, R. A.; Adkins, N.; Woodcock, C. L.; Wade, P. A.; Hansen, J. C. *J. Biol. Chem.* **2003**, *278*, 32181

26. Chandler, S. P.; Guschin, D.; Landsberger, N.; Wolffe, A. P. *Biochemistry*, **1999**, *38*, 7008

27. Ha, T. *Methods*, **2001**, *25*, 78

28. Clegg, R. M. *Methods Enzymol.* **1992**, *211*, 353

29. Stryer, L.; Haugland, R. P. *Proc. Natl. Acad. Sci. USA*, **1967**, *58*, 719

30. McKinney, S. A.; Declais, A.-C.; Lilley, D. M. J.; Ha, T. *Nat. Struct. Biol.* **2003**, *10*, 93

31. Forster, T. *Naturwissenschaften*, **1946**, *33*, 166

32. Mujumdar, R. B.; Ernst, L. A.; Mujumdar, S. R.; Lewis, C. J.; Waggoner, A. S. *Bioconjug. Chem.* **1993**, *4*, 105

33. Zheng, H. C.; Tomschik, M.; Zlatanova, J.; Leuba, S. H. in: Golemis, E.; Adams, P. (Eds.), *Protein-Protein Iteractions, A Molecular Cloning Manual*, 2nd ed. Cold Spring Harbor Laboratory Press, Cold Spring Harbor, **2005**, pp. 429-444

34. Harada, Y.; Sakurada, K.; Aoki, T.; Thomas, D. D.; Yanagida, T. *J. Mol. Biol.* **1990**, *216*, 49

35. McKinney, S. A.; Tan, E.; Wilson, T. J.; Nahas, M. K.; Declais, A. C.; Clegg, R. M.; Lilley, D. M.; Ha, T. *Biochem. Soc. Trans.* **2004**, *32*, 41

36. Zhuang, Z.; Kim, H.; Pereira, M, J.; Babcock, H. P.; Walter, N. G.; Chu, S. *Science,* **2002**, *296*, 1473

37. Zhuang, Z.; Bartley, L. E.; Babcock, H. P.; Russell, R.; Ha, T.; Herschlag, D.;Chu, S. *Science,* **2000**, *288*, 2048

38. Kim, H. D.; Nienhaus, G. U.; Ha, T.; Orr, J. W.; Williamson, J. R.; Chu, S. *Proc. Natl. Acad. Sci. USA,* **2002**, *99*, 4284

39. Ha, T.; Ting, A. Y.; Liang, J.; Caldwell, W. B.; Deniz, A. A.; Chemla, D. S.; Schultz, P. G.; Weiss, S. *Proc. Natl. Acad. Sci. USA,* **1999**, *96*, 893

40. Axelrod, D. *Methods Cell Biol.* **1989**, *30*, 245

41. Funatsu, T.; Harada, Y.; Tokunaga, M.; Saito, K.; Yanagida, T. *Nature,* **1995**, *374*, 555

42. Tan, E.; Wilson, T. J.; Nahas, M. K.; Clegg, R. M.; Lilley, D. M. J.; Ha, T. *Proc. Natl. Acad. Sci. USA,* **2003**, *100*, 9308

43. Ransik, I.; McKinney, S. A.; Ha, T. *Nat. Methods*, **2006**, *3*, 891

44. Koopmans, W. J. A.; Brehm, A.; Logie, C.; Schmidt, T.; Noort, J. van, *J. Fluoresc.* **2007**, *17*, 785